

---

# Nuclear Magnetic Resonance Proton Imaging of Bone Pathology

H. Atlan, R. Sigal, H. Hadar, R. Chisin, I. Cohen, A. Lanir, M. Soudry, Y. Machtey, R. Schreiber, and J. Benmair

*Medical Biophysics Department, Hadassah University Hospital, Jerusalem; Radiology and Orthopaedics Departments, Beilinson Hospital, Petach Tikva; Orthopaedics and Biochemistry Departments, Rothschild Medical Centre, Haifa; and Elscint MRI Center, Herzlia, Israel*

Thirty-two patients with diversified pathology were examined with a supraconductive NMR imager\* using spin echo with different TR and TE to obtain  $T_1$  and  $T_2$  weighted images. They included 20 tumors (12 primary, eight metastasis), six osteomyelitis, three fractures, two osteonecrosis, and one diffuse metabolic (Gaucher) disease. In all cases except for the stress fractures, the bone pathology was clearly visualized in spite of the normal lack of signal from the compact cortical bone. Nuclear magnetic resonance (NMR) imaging proved to be at least as sensitive as radionuclide scintigraphy but much more accurate than all other imaging procedures including computed tomography (CT) and angiography to assess the extension of the lesions, especially in tumors extended to soft tissue. This is due both to easy acquisition of sagittal and coronal sections and to different patterns of pathologic modifications of  $T_1$  and  $T_2$  which are beginning to be defined. It is hoped that more experience in clinical use of these patterns will help to discriminate between tumor extension and soft-tissue edema. We conclude that while radionuclide scintigraphy will probably remain the most sensitive and easy to perform screening test for bone pathology, NMR imaging, among noninvasive diagnostic procedures, appears to be at least as specific as CT. In addition, where the extension of the lesions is concerned, NMR imaging is much more informative than CT. In pathology of the spine, the easy visualization of the spinal cord should decrease the need for myelography.

J Nucl Med 27:207-215, 1986

---

Conventional and radiology tomographies were the techniques of choice to visualize bone pathology with a relatively high resolution. This is due to the high absorption coefficient and the relatively small individual variations of bone structures. More recently, the use of body computed tomography (CT) (1-3) has allowed for very accurate localization of bone tumors and inflammatory diseases. Similarly, CT has proven to be very useful for the diagnosis of fractures in problematic anatomic regions. Moreover, the introduction of body CT in bone tumors has considerably decreased the need for arteriography in order to assess the extension of the disease to soft tissues. For this reason, radionuclide scintigraphies were not considered very useful for bone pathology until it was found that their sensitivity may

be much higher for the diagnosis of most bone diseases, although their specificity and anatomic resolution are lower. This is because they display physiologic processes rather than plain morphology.

Similarly, it was thought at the beginning that proton nuclear magnetic resonance (NMR) would not prove to be useful for bone pathology, especially in view of the fact that cortical bones do not produce signals under the field and pulse conditions generally used. However, because of the high anatomic resolution in medullary bone visualization including sagittal and coronal sections, and because of the chemical and physiologic resolution expected as a result of the sensitivity of NMR signals to  $T_1$  and  $T_2$  relaxation processes, NMR proton imaging of bones seems to be a very valuable procedure (4-7,9). The purpose of this work was to compare the information obtained by NMR proton imaging with that obtained by other imaging procedures in order to assess its place in the clinical work-up of bone pathology. To do this we studied a limited number of patients with diversified bone pathology.

---

Received Apr. 15, 1985; revision accepted Nov. 1, 1985.  
For reprints contact: H. Atlan, MD, PhD, Medical Biophysics Dept., Hadassah University Hospital, Jerusalem, Israel.

**TABLE 1**  
Various Bone Diseases Examined by NMR Proton Imaging and Other Imaging Procedures in Present Study

Patient no.	Item	X-ray	Nuclear medicine	CT	Angiography	Biopsy	MRI
1	Osteogenic sa. femur	+	+	+		+	+
2	Osteogenic sa. femur	±†	+	+	+	+	+
3	Osteogenic sa. femur	+	+	+	+	+	+
4	Osteogenic sa. tibia	+	+	+	+	+	+
5	Ewing sa. fibula	+	+	+		+	+
6	Ewing sa. fibula	+	+	+		+	+
7	Ewing sa. tibia	+	+	+		+	+
8	Eosinophilic granuloma cranial vault	+	-			+	+
9	Eosinophilic granuloma humerus	+	+	+		+	+
10	Osteoid osteoma fibula	+	+				+
11	Hemangioma mandibula	+	+	+	+		+
12	Cyst trochanter	-‡	+	-	+		+
13	Metastasis (prostate) femur	+	+			+	+
14	Metastasis (lung oat cell ca.) femur	+	+				+
15	Metastasis (fibro sa.) knee (mostly soft tissue)	-	-	-	+		+
16	Metastasis (breast) spine with mild chord compression	±	+				+
17	Metastasis (bladder) spine	-	+				+
18	Metastasis (breast) spine	-	+	-			+
19	Metastasis (breast) spine	±	+				+
20	Metastasis (breast) spine	+	+				+
21	Osteonecrosis femoral condyle	±	+				+
22	Osteonecrosis femoral condyle	±	+				+
23	Acute osteomyelitis L5	+	+				+
24	Acute osteomyelitis post knee replacement	-	+				+
25	Acute osteomyelitis femur	-	-				+
26	Acute osteomyelitis acetabulum	-	+	-			+
27	Acute osteomyelitis head of femur	+	+				+
28	Chronic osteomyelitis femur	+	+	+			+
29	Fracture C5	+	-				+
30	Stress fracture femur	+	+				-
31	Stress fracture femur	+	+			+	-§
32	Gaucher disease	-				+	+

\* +: Pathologic finding.

† ±: Doubtful.

‡ -: Normal.

§: No pathologic finding in bony structures but modified signal intensity in surrounding soft tissue.

## MATERIALS AND METHODS

### Patient Population

NMR images of the skeletal system were obtained in 32 patients ranging in age from 15-72 yr. Informed consent was obtained in all cases. The diagnoses included bone tumors (primary and metastatic), osteonecrosis, osteomyelitis, fractures, and metabolic diseases (Table 1). All patients had other imaging studies within

2 wk of NMR, including conventional x-ray, bone scintigraphy, CT, or arteriography. The results of the clinical and imaging data were correlated with findings at surgery and biopsy.

### Imaging Techniques

Magnetic resonance imaging (MRI) was performed with a superconducting magnet† operating at 0.5T (21.3 mHz). For spine imaging an elliptical body coil was used with a 57 × 37-cm aperture and 60-cm length.

A circular coil 27 cm in diam and 28 cm in length was used for limbs. All images were obtained using a two-dimensional Fourier transform technique (2DFT). Data were collected on a  $256 \times 128$  or  $256 \times 256$  matrix and interpolated to a  $512 \times 512$  matrix for display. Slice thickness varied from 5 to 10 mm and sequential imaging slices were typically 2 or 3 mm apart. Imaging was obtained in direct axial, coronal, and sagittal planes. A multi-echo, multislice imaging technique was used and the total number of slices per scan depended upon the scan protocol (8 or 17 min for scanning 20 slices). All images were obtained from spin echoes (SE) with echo delay times (TE) of 28.5 and 70 msec (first and second echo, respectively). The repetition time per cycle (TR) varied from 500 msec to 2,000 msec; in most cases averaging two signals was sufficient to get a good signal-to-noise ratio. Every patient was imaged using at least two different planes and two different TR, so as to obtain  $T_1$  weighted images (short TR and TE) and  $T_2$  weighted images (long TR and TE). Thus,  $T_1$  and  $T_2$  relaxation times could be estimated from the intensity data, using the method of Herfkens et al. (8). This method uses the ratio of intensities produced by different TR to calculate  $T_1$ , and different TE to calculate  $T_2$ . Intensity measurements of different tissues within the same image or from one image to another can be compared if standardization is performed using an external (phantom) or internal reference standard (paraspinomuscles in this study).

## RESULTS

### Neoplasmas

Four patients had osteogenic sarcomas (three femur, one tibia). The diagnosis was based on open biopsy (followed in one case by surgical removal) with gross and microscopic examination. Bone tumors were clearly demonstrated using long or short TR. In all cases they appeared to be unhomogeneous with a general trend towards decreased intensity on  $T_1$  weighted images (long  $T_1$ ) and increased intensity on  $T_2$  weighted images (long  $T_2$ ). In addition, a striking fact was noted: The existence of very low intensity areas within the tumor visible in all pulse sequences. Correlation with pathologic examinations made it possible to establish that these areas corresponded to cortical-like mineralized, calcified parts of the tumors and the low intensity signal was due to a decrease in mobile proton density as expected in newly formed compact bone. The cortical outline of the bone was destroyed in three cases and the upper extension of the tumor was clearly depicted on the longitudinal slices (Fig. 1). In all cases the maximum extension in the soft tissues was noted, and its limits clearly delineated although it is not yet possible

to differentiate it from edema with certainty.

In three patients with Ewing's tumor (two fibula, one tibia) the  $T_2$  weighted images demonstrated a region with very high intensity signals located at the cortical part of the bone with limited bone marrow involvement. Extension to the soft tissues was readily checked (Fig. 2). In two cases, MRI scans were performed after radiotherapy showing a nearly total disappearance of the mass which was confirmed by biopsy.

Two patients with eosinophilic granuloma were studied (one humerus, one cranial vault). In both cases prolonged  $T_2$  and reduced  $T_1$  were noted (Fig. 3).

In one patient with osteoid osteoma (fibula) a global enlargement of the head of the fibula without rupture of the cortical bone was observed.

One patient presented with a hemangioma of the mandibula. Disruption of the mandibula at different levels was noted; the tumor produced a high intensity signal on the  $T_2$  weighted image (Fig. 4). A cyst of the left trochanter appeared on MRI as an oval circumscribed lesion with no cortical rupture and no peripheral reaction (Fig. 5).

Eight patients presented with metastatic tumors from breast, prostate, bladder, and lung primaries. The femur was involved in two cases, the spine in six cases. Metastases usually appeared as masses with a low intensity (Fig. 6) on both  $T_1$  and  $T_2$  weighted images but some lesions demonstrated an increased intensity, especially on  $T_2$  weighted images. This variability may be due to the different origins of the primary tumors or to a different ratio between osteoblastic and osteolytic reactions according to the rationale mentioned above on differences in patterns of signal intensities within osteogenic sarcoma.

In tumors of the spine, sagittal scans were particularly important in order to check the integrity of the spinal cord and they prevented the need for myelography (plain or with CT). Because of the low intensity of CSF on  $T_1$  weighted images, it was not always possible to differentiate it from the cortex of the vertebral bodies. However, on  $T_2$  weighted images, increased TR and TE values allowed for clear differentiation between them, since cortical bone remains dark and CSF becomes bright (Fig. 7).

Osteonecrosis of the femoral condyle (Fig. 8) was clearly demonstrated in two cases. The relationship with intracapsular structures was observed. Five cases of acute osteomyelitis were studied. The femur was involved in three cases, the acetabulum in one and the lumbar spine in one. One patient presented a postoperative infection or loosening and he was checked after the removal of the femoral prosthesis. Replacement of the bone marrow by abnormal tissue was seen in all cases (Fig. 9B). Prolonged  $T_1$  was observed. One case of chronic osteomyelitis of femur metaphysis was imaged; it was characterized by a femoral shaft deformation,

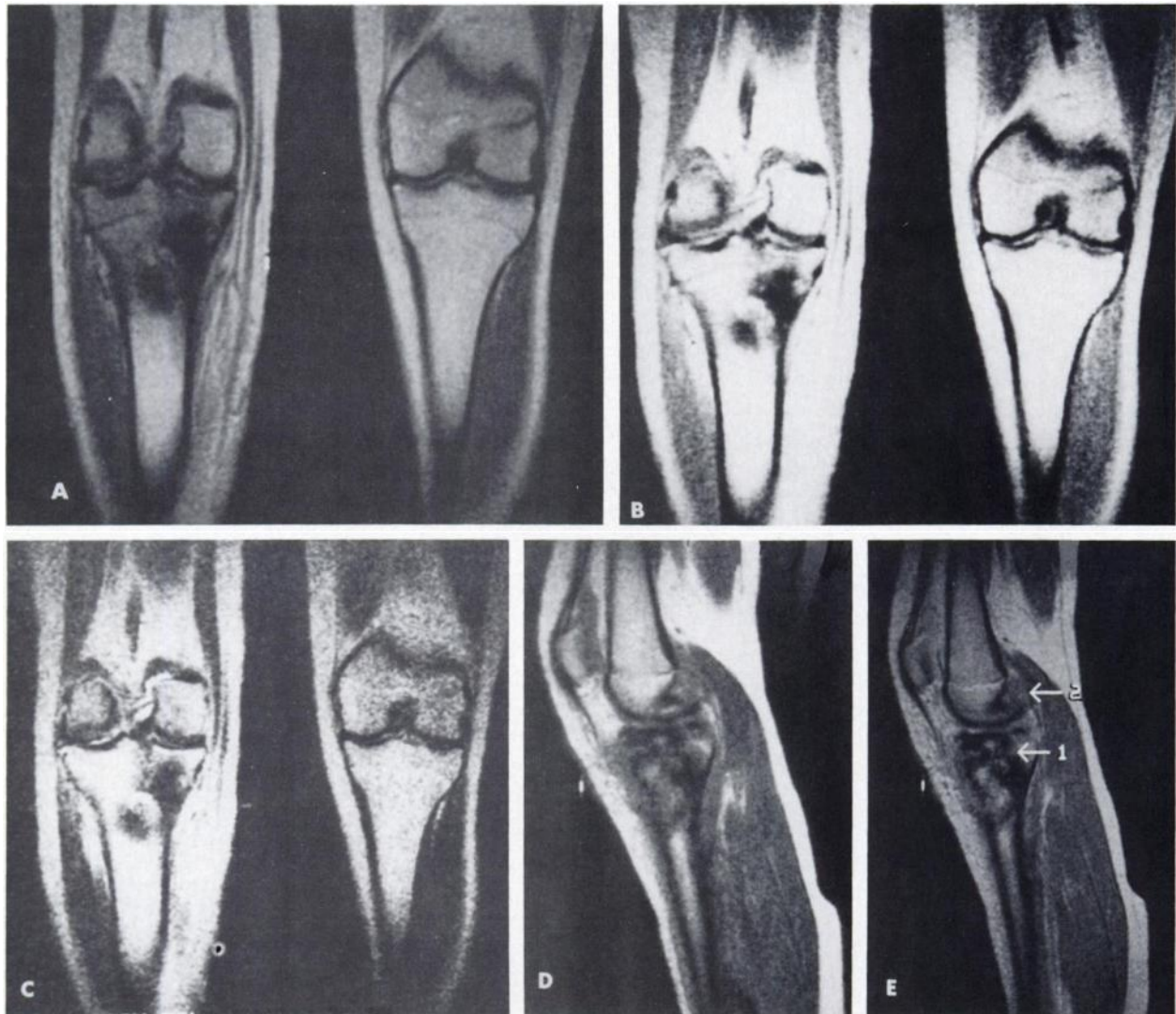


**FIGURE 1**

Coronal section of osteogenic sarcoma of right tibia. A: Spin-echo  $T_1$  weighted image (TR: 563 ms; TE: 28.5 ms) with reduced signal (long  $T_1$ ) as compared with normal tissue in left tibia. B: Long TR (1,850 ms) first echo (TE: 28.5 ms); and C: Second echo ( $T_2$  weighted image 1,850/75 ms) showing increased signal in tumor (long  $T_2$ ) except for two black regions with no signal. The same regions did not show any detectable signal in pictures obtained by all other pulse sequences, as is the case in cortical bone. They correspond to newly formed compact tumoral bone; D and E: Spin echo (563/28.5 ms and 1,850/28.5 ms, respectively) sagittal section in central part of right knee between femoral condyles. First arrow indicates tumor. Extension can be noticed to soft tissue anteriorly but not to upper border of tibia and articulation interline, as verified by pathologic examination after amputation. Second arrow shows normal intercondyle formations which should not be confused with extension to femur

cortex thickening and bone marrow involvement (Fig. 9A). A post-traumatic fracture of the body of C5 was identified as a modified morphology without a change in signal intensity as compared with adjacent vertebrae. The absence of displacement was easily verified.

Two stress fractures of the femur were documented by x-rays and radionuclide scintigraphy and could not be seen by NMR. One of them was suspected of being a malignant tumor on the basis of x-rays and scintigra-

phy. The NMR findings, where an extended pathology was found in the surrounding muscle but not in the bone, did not support the diagnosis of tumor (Fig. 10). The biopsy and evolution ruled it out.

One patient with Gaucher disease was imaged and the involvement of the whole femur and tibia was demonstrated; the whole bone marrow appeared to have been replaced by abnormal tissue with decreased intensity on both  $T_1$  and  $T_2$  images indicating long  $T_1$  and short  $T_2$  values. This abnormal tissue was located at the

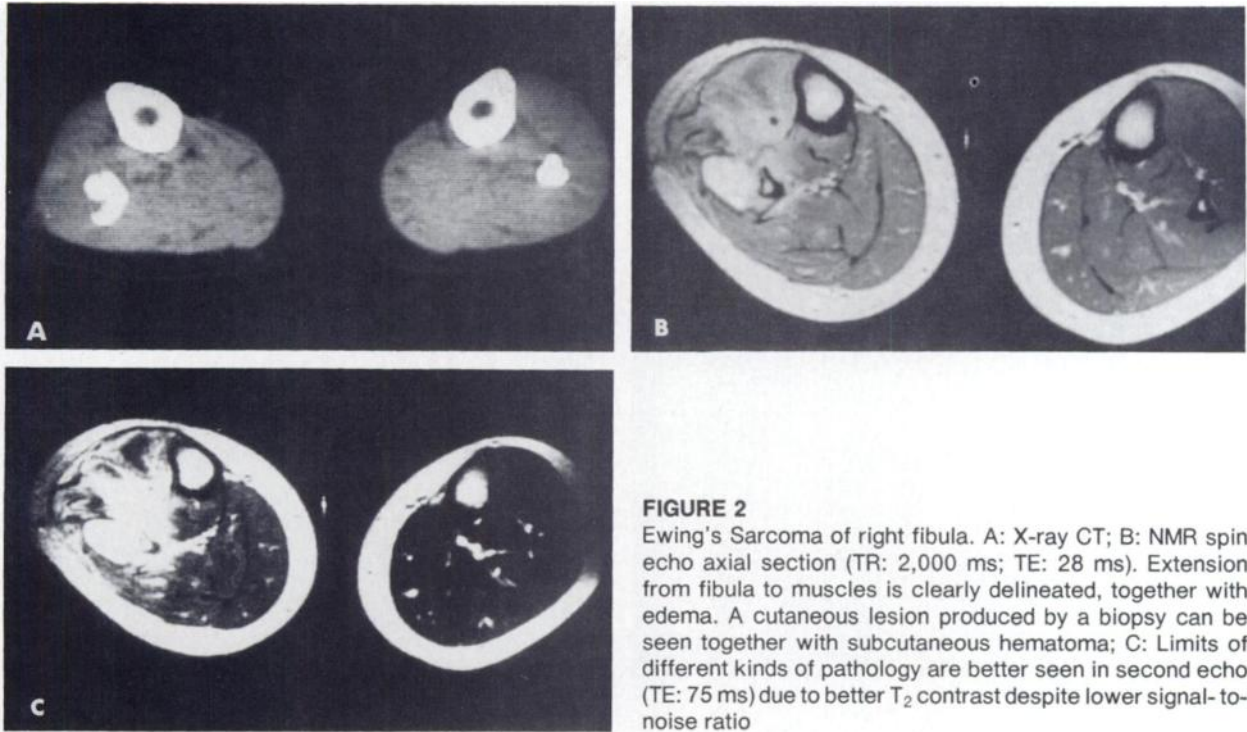


**FIGURE 2**  
Ewing's Sarcoma of right fibula. A: X-ray CT; B: NMR spin echo axial section (TR: 2,000 ms; TE: 28 ms). Extension from fibula to muscles is clearly delineated, together with edema. A cutaneous lesion produced by a biopsy can be seen together with subcutaneous hematoma; C: Limits of different kinds of pathology are better seen in second echo (TE: 75 ms) due to better  $T_2$  contrast despite lower signal-to-noise ratio

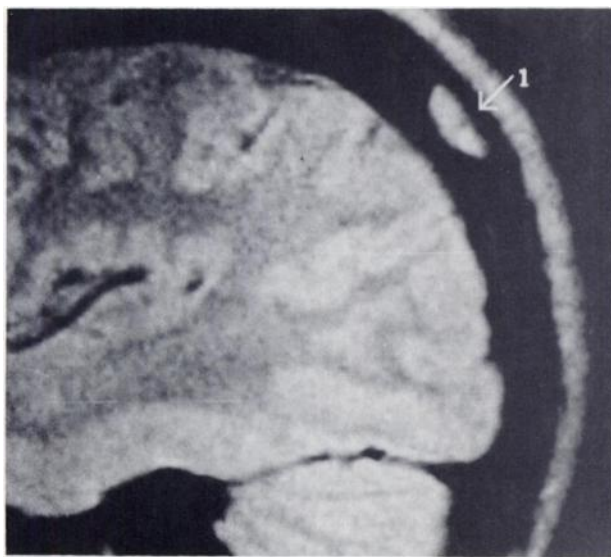
level of the metaphysis, the epiphysis being preserved (Fig. 11).

Table 1 shows the results of the various imaging procedures performed on the patients in this study. In all cases of tumors and osteomyelitis of long bones, NMR imaging confirmed the anatomic findings of conventional x-rays and CT with additional information due to the combination of high pathologic resolu-

tion and ease in obtaining sagittal and coronal views.

#### DISCUSSION

A preliminary characterization of patterns of signal intensities in  $T_1$  and  $T_2$  weighted images could be described in different bone tumors. As shown in our results, a difference between regions of decreased signal



**FIGURE 3**  
Eosinophilic granuloma of cranial vault (TR: 1,850 ms; TE: 28 ms)

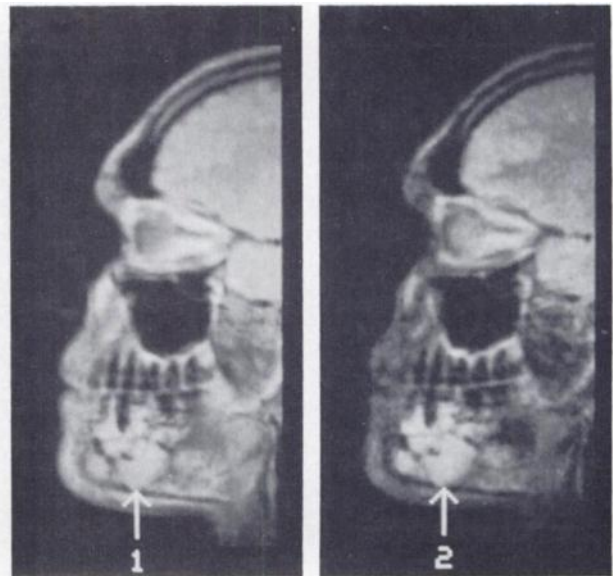


**FIGURE 4**  
Hemangioma of mandibula with clear delineation of extension of lesions, especially in second echo by making use of its high  $T_2$  contrast

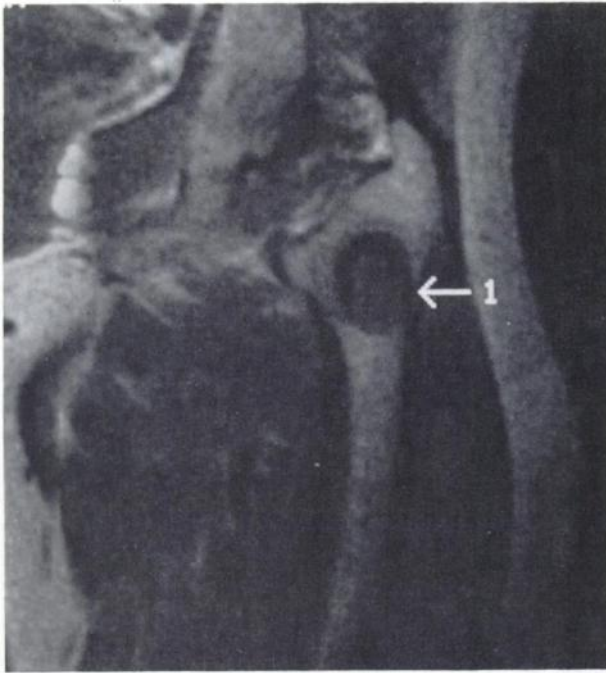


**FIGURE 5**  
Cyst of left trochanter (TR: 500 ms; TE: 28.5 ms)

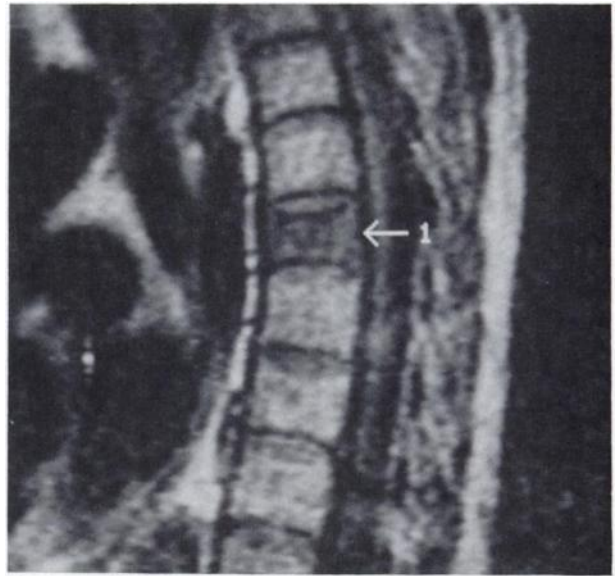


**FIGURE 6**  
Spin-echo T<sub>1</sub> weighted image (337/29 ms) showing meta-  
static lesion of the whole vertebral body (D6) with increased  
T<sub>1</sub>

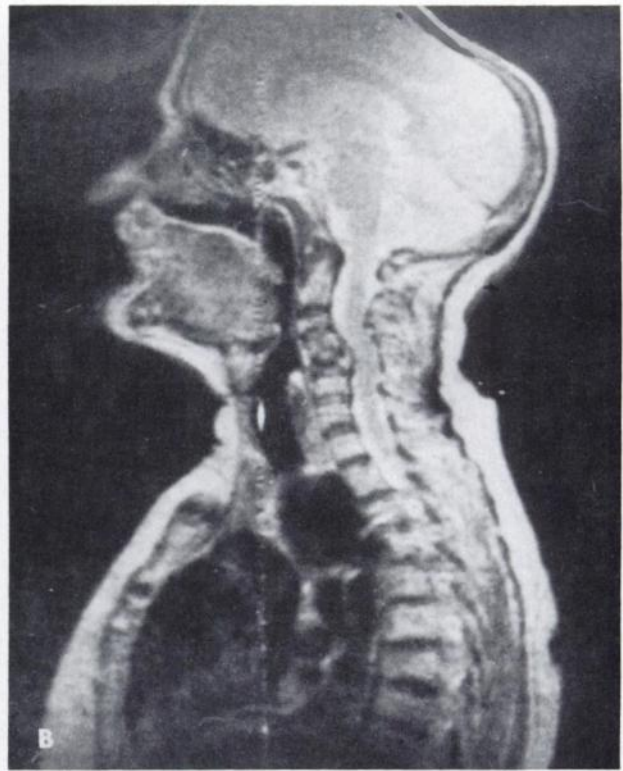
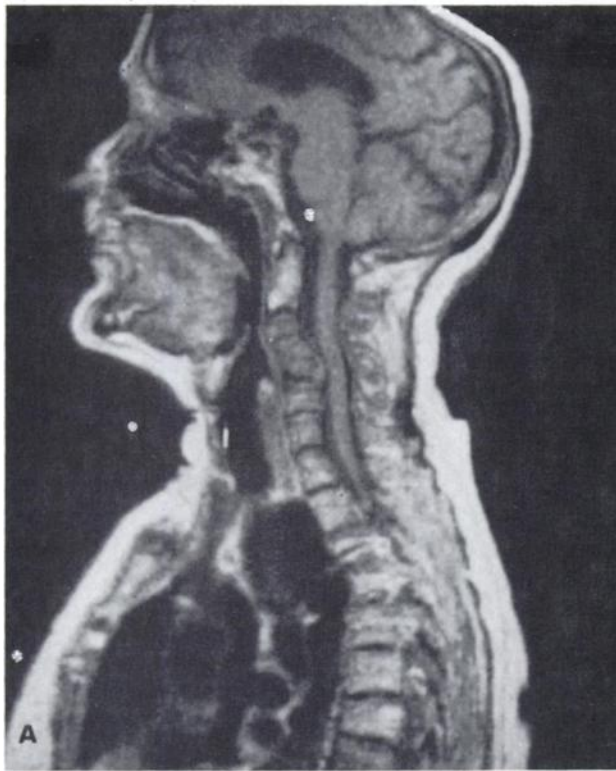


**FIGURE 7**  
Metastatic lesion of Case 3 and Case 4 with cord compression. A: T<sub>1</sub> weighted image (500/28.5 ms). B: T<sub>2</sub> weighted image (2,000/57 ms) allows clear differentiation of perimedullary space with CSF (in white) from compact cortical bone which remains black whatever pulse sequence may be. Notice regions with low signal intensity (black) within lesions in both T<sub>1</sub> and T<sub>2</sub> weighted images, suggesting low mobile proton density as in compact bone and osteoblastic reaction

intensities in  $T_1$  and  $T_2$  weighted images and regions with increased signal in  $T_2$  weighted images and decreased signal in  $T_1$  weighted images is likely to correspond to either osteoblastic or osteolytic reactions respectively; the former would produce a decreased mobile proton density in regions of compact bone neoformation, while the latter, replacing the normal tissue by the tumor, would result in longer  $T_1$  and  $T_2$ . Whether this pattern will be specific enough to differentiate between osteoblastic reactions with bone neoformation and osteolytic reactions remains to be established.

In the assessment of tumors, comparison with CT (and even angiographies) shows that NMR is the superior imaging modality for demonstrating the extension to soft tissues and its limits. In CT, although a decrease in density is noted in the muscular extension of the tumor, no clear cut limits with normal muscle can be distinguished (Fig. 2), while very clear limits can be seen in the NMR images. However, the size of these limits varies depending on the used pulse sequence. This may be due to different signals coming from tumoral tissue as compared with adjacent muscle oedema.

It is hoped that when a better pathologic resolution between tumor tissue and edema is obtained by differentiation based on  $T_1$  and  $T_2$  measurements, and/or associated metabolic spectroscopy, NMR imaging will provide the information on the exact extension of the tumors still needed by the surgeon for a confident planning of the treatment.

One case of osteomyelitis (Fig. 11) was of particular interest since the known pathology was chronic osteo-

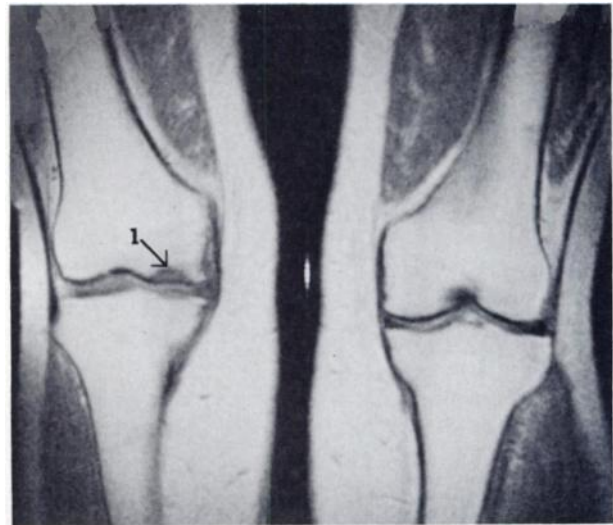


**FIGURE 8**  
 $T_1$  weighted image (556/28 ms) of osteonecrosis in right medial condyle

myelitis in the left femur and was easily visualized on NMR, while a hidden unsuspected focus of acute osteomyelitis was found in the right femur and confirmed by clinical (poor) symptomatology and technetium-99m methylene diphosphonate scintigraphy.

In fractures, the lack of NMR signal intensity changes in bony structures may be a useful tool to differentiate between tumor and stress fracture in the presence of clearly positive scintigraphies (with or without x-ray findings) as reported above. On the basis of

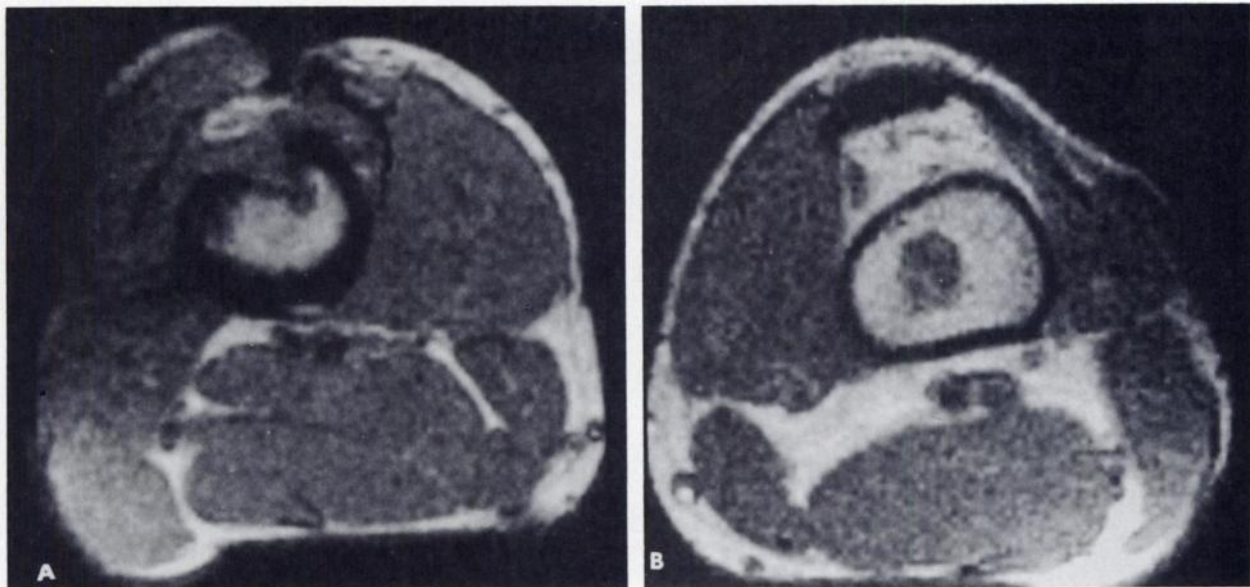


**FIGURE 9**  
 Spin-echo (911/28 ms) axial sections of thighs. A: Chronic osteomyelitis of left femur produces enlargement of cortical bone with decreased nonhomogeneous signal in medulla. B: In right femur of same patient acute osteomyelitis appears as cavity within medullary bone

the one case of Gaucher disease the usefulness of NMR imaging for bone metabolic diseases seems promising. In all these cases the radionuclide scintigraphies were clearly pathological although nonspecific, as is well known.

In conclusion, despite the limitations due to the absence of signal from the compact cortical bone, NMR proton imaging of long bones (in addition to the spine) proved to be a useful diagnostic procedure to assess the extent of lesions. It is likely that it will prove to be even more useful when a better discrimination between different pathologies becomes possible on the basis of different patterns of  $T_1$ ,  $T_2$ , and proton density modifications

as well as association with metabolic spectroscopy.

Thus, radionuclide scintigraphy, remaining the most sensitive and easy to perform test, especially in malignant tumors and stress fractures, will remain a screening procedure, complemented by conventional x-rays. Since NMR achieves no less specificity than CT scanning in bone tumors and inflammatory diseases and achieves much more sensitivity regarding soft tissues, NMR seems to be the procedure of choice for a better delineation of the lesions. Because of potential hazards of ionizing radiation, especially in children, it is likely that additional CT imaging will not be necessary in most cases.

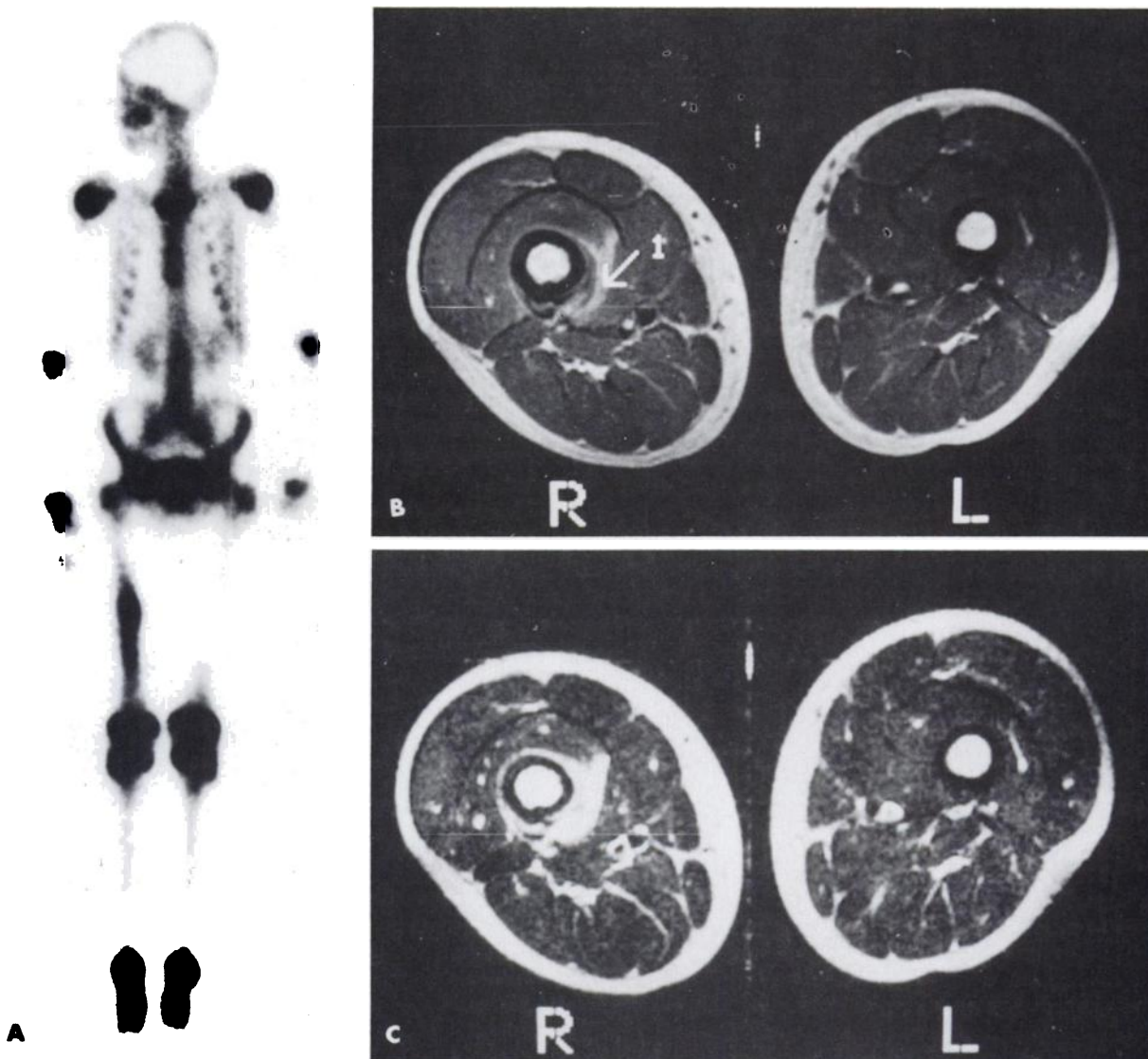


**FIGURE 10**

Stress fracture of right femur. A: Intense focus of pathological uptake in [ $^{99m}\text{Tc}$ ]MDP scintigraphy. This finding, together with x-rays, raised high suspicion of malignancy; however, a negative biopsy and return to normal ruled it out and confirmed diagnosis of stress fracture. B and C: NMR images (spin echo 2,000/28 and 70 ms) did not show any abnormal signal from bone structures; however, region of intense signal can be seen in adjacent soft tissue with even more contrast in second echo picture, indicating an edematous region with prolonged  $T_2$

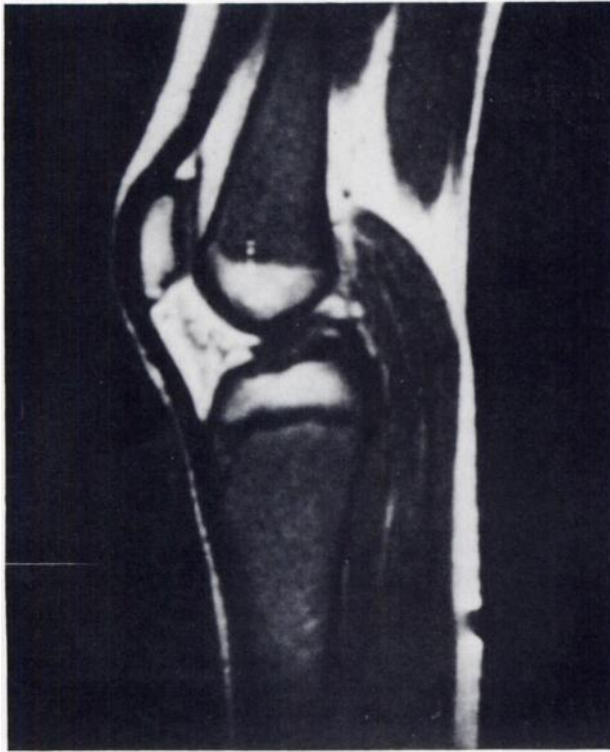


**FIGURE 11**  
Gaucher disease. Whole medullary bone of femur and tibia appears with much lower signal than normal ( $T_1$  weighted image 556/28 ms). Same finding was observed in  $T_2$  weighted image (2,000/70 ms) indicating replacement of medullar tissue by abnormal one with longer  $T_1$  and  $T_2$

## FOOTNOTE

\* Elscint, Inc., Boston, MA (0.5 Tesla).

† Elscint, Inc., Boston, MA (Gyrex S-5000).

## REFERENCES

1. Wilson JS, Korobkin M, Genant HK, et al: Computed tomography of musculoskeletal disorders. *Am J Roentgenol* 131:55-61, 1978
2. deSantos LA, Goldstein HM, Murray JA, et al: Computed tomography in the evaluation of musculoskeletal neoplasms. *Radiology* 128:89-94, 1978
3. Riddlesberger MM: Computed tomography of the musculoskeletal system. *Rad Clin North Am* 19:463-477, 1981
4. Brady TJ, Gebhardt MC, Pykett IL, et al: NMR imaging of forearms in healthy volunteers and patients with giant-cell tumor of bone. *Radiology* 144:549-522, 1982
5. Moon KL, Genant HK, Helms CA, et al: Musculoskeletal applications of NMR. *Radiology* 147:161-171, 1983
6. Brady TJ, Rosen BR, Pykett IA, et al: NMR imaging of leg tumors. *Radiology* 149:181-187, 1983
7. Cohen DC, Klatte EC, Baehner R, et al: MRI of bone marrow diseases in children. *Radiology* 151:715-718, 1984
8. Herfkens R, Davis P, Crooks LE, et al: NMR imaging of the abnormal live rat and correlations with tissue characteristics. *Radiology* 141:211-218, 1981
9. Totty WJ, Murphy WA, Ganz WI, et al: Magnetic resonance imaging of the normal and ischemic femoral head. *Am J Roentgenol* 143:1279-1280, 1984